Earth's dynamo limit of predictability

G. Hulot,[1] F. Lhuillier,[1,2] and J. Aubert[2]

Received 20 November 2009; revised 22 January 2010; accepted 19 February 2010; published 25 March 2010.

[1] Earth's magnetic field is currently decreasing, reducing the protection it offers against charged particles coming from space and increasing space weather hazards within the near-Earth environment. Modeling the future evolution of the field is thus of considerable interest. But how far in the future this can conceivably be done is still an open question. Here we report on the first systematic investigation of the limit of predictability of fully consistent 3D numerical dynamo simulations, and suggest that the Earth's dynamo is likely unpredictable beyond a century, making decade timescale forecasts of the main magnetic field conceivable, but rendering longer-term predictions, such as the timing of the next reversal, totally unpredictable. **Citation:** Hulot, G., F. Lhuillier, and J. Aubert (2010), Earth's dynamo limit of predictability, *Geophys. Res. Lett.*, *37*, L06305, doi:10.1029/2009GL041869.

1. Introduction

[2] The main magnetic field produced by the geodynamo within the Earth's liquid core provides a very effective shield against the energetic charged particles that come from the Sun and space [*Lundin et al.*, 2007]. It is also an essential ingredient in defining the near-Earth space weather conditions within which satellites orbit [*Baker*, 2002]. Its intensity is however known to decrease significantly at present, especially in the so-called South-Atlantic Anomaly, where the low value of the field is already an issue to space technology [*Heirtzler*, 2002]. Whether this trend will last for some time, enhance space weather hazards on the decade timescale and possibly lead to a reversal of the field on the millennium timescale, is a question that forecasting strategies of the type commonly used in meteorology [*Kalnay*, 2003] could possibly answer. Such strategies start developing in the context of geodynamo assimilation [*Fournier et al.*, 2007; *Kuang et al.*, 2008]. But just as for meteorology, forecasts will inevitably be limited in time by the nonlinear nature of the governing equations, as the geodynamo unfortunately belongs to the same class of non-periodic dynamical systems that can exhibit chaotic behavior.

[3] Although some attempts have been made to characterize this system as such, using either a complex generalization of *Lorenz*'s [1963] equations [*Jones et al.*, 1985], or a turbulent mean-field dynamo model [*Ryan and Sarson*, 2008], no investigation of the finite limit of predictability of the fully consistent 3D magnetohydrodynamic equations that govern it has yet been carried out. Appropriate geodynamo simulation codes have however been available for a little more than a decade [*Glatzmaier and Roberts*, 1995], leading to substantial progress in our understanding of the physical mechanisms at work [*Christensen and Wicht*, 2007] and of what may be responsible for the current decrease of the main field [*Hulot et al.*, 2002]. This prompted us to investigate the finite limit of predictability of such dynamos, taking advantage of the now relatively accessible CPU time those codes require to run.

2. Numerical Models and Relevant Parameters

[4] In our simulations, the dynamo is assumed thermally driven, with fixed and homogeneous temperatures imposed at both the inner-core and core-mantle boundaries. The electrically conducting inner core (with the same conductivity as the liquid core) is free to rotate (along the Earth's rotation axis) with respect to the electrically insulating mantle, and mechanical boundary conditions are assumed rigid at both boundaries. Each simulation can then entirely be defined by four dimensionless control parameters [*Christensen and Aubert*, 2006]: the modified Rayleigh number $Ra^* = \alpha g_0 \Delta T/\Omega^2 D$, the Ekman number $E = \nu/\Omega D^2$, the Prandtl number $Pr = \nu/\kappa$, and the magnetic Prandtl number $Pm = \nu/\eta$ (with α the thermal expansion coefficient; g_0 the gravity at the core-mantle boundary; ΔT the temperature difference between the inner and outer boundaries; Ω the Earth's rotation rate; D the difference between the inner-core and outer-core radii; ν, the kinematic viscosity; κ and η the thermal and magnetic diffusivities of the core).

[5] Unfortunately no such simulation can yet be run with what are believed to be relevant parameter values for the Earth's dynamo [*Christensen and Wicht*, 2007] (roughly $E = 10^{-15} - 10^{-14}$, $Pr = 0.1 - 1$ and $Pm = 10^{-6} - 10^{-5}$, as inferred from the known physical properties of the mainly iron alloy core, though E could be as large as 10^{-9} if turbulent viscosity is taken into account [*Roberts*, 2007]), the value of Ra^* being essentially unknown (save that it must be well beyond the critical number required for dynamo action). This limitation can however be obviated by running a large number of numerically accessible dynamo simulations, identifying underlying physical mechanisms, and inferring scaling rules that can hopefully be extrapolated to the Earth case, a strategy that has already been extensively discussed, met with some success [*Christensen and Aubert*, 2006; *Christensen and Tilgner*, 2004], and which we will therefore use.

[6] For that purpose, another dimensionless parameter turns out to be very useful: the Reynolds number $Rm = U_0 D/\eta$ (U_0 being the RMS value of the flow velocity within

[1]Equipe de Géomagnétisme, Institut de Physique du Globe de Paris, Université Paris-Diderot, INSU, CNRS, Paris, France.
[2]Equipe de Dynamique des Fluides Géologiques, Institut de Physique du Globe de Paris, Université Paris-Diderot, INSU, CNRS, Paris, France.

0094-8276/10/2009GL041869

the dynamo), which can be seen as the ratio $Rm = \tau_D / \tau_T$ of the magnetic diffusive time $\tau_D = D^2/\eta$ to the turnover time $\tau_T = D/U_0$. For the Earth $D \approx 2260$ km, $\tau_D \approx 120$ kyr (assuming $\eta = 1.32\ m^2\ s^{-1}$ as *Christensen and Tilgner* [2004]) and Rm is on order $Rm = 10^2 - 10^3$ [*Christensen and Wicht*, 2007]. Contrary to the control parameters E, Pr, Pm, and Ra*, Rm is not a number that can be set a priori in dynamo simulations. Rather, it comes as an output of the simulations. But in varying the control parameters one can easily ensure that a wide range of Rm values is produced.

[7] In practice, our dynamo simulations were obtained by solving equations (2)–(5) of *Christensen and Aubert* [2006] and running the code of *Aubert et al.* [2008] (an evolution of the ACD code benchmarked by *Christensen et al.* [2001]), which uses spherical coordinates (r, θ, φ) and a semi-spectral method, with spherical harmonics $Y_n^m(\theta, \varphi)$ expansions and a second-order finite-differencing scheme in the radial direction (with geometrical progression towards the boundaries to resolve boundary layers). Solutions at time t were thus defined by five scalar functions of the form $X(r,\theta,\varphi,t) = \sum_{n,m} x_n^m(r,t) Y_n^m(\theta,\varphi)$: two for the poloidal and toroidal components of the flow, two for the poloidal and toroidal components of the magnetic field, and one for the temperature field. Resolution varied between 44 and 106 in spherical harmonic degree, and 90 and 160 in radial grid points, depending on the simulation, to ensure convergence.

3. Error Growth in Perturbed Dynamo Simulations

[8] Our investigation of the limits of predictability of those dynamos began with the production of 30 reference simulations, each with different sets of control parameters (see Figures 1–3). For each reference simulation, we next closely followed the approach originally used in meteorology [*Lorenz*, 1965; *Charney et al.*, 1966; *Kalnay*, 2003]. This consists in slightly perturbing the system in a perfectly controlled way at a known time, and comparing the subsequent evolution of the perturbed simulation with respect to the reference one.

[9] We were careful to ensure that simulations could be stopped and restarted without introducing rounding errors, and introduced perturbations of controlled relative magnitude ε at times t_p in the following ways: either in just the axial dipole poloidal magnetic field (changing the corresponding $x_1^0(r, t_p)$ values into $\tilde{x}_1^0(r, t_p) = x_1^0(r, t_p)(1 + \varepsilon)$), or in all harmonics of one of the $X(r,\theta,\varphi,t)$ functions defining the magnetic, flow or temperature fields (changing all the corresponding $x_n^m(r, t_p)$ values into $\tilde{x}_n^m(r, t_p) =$

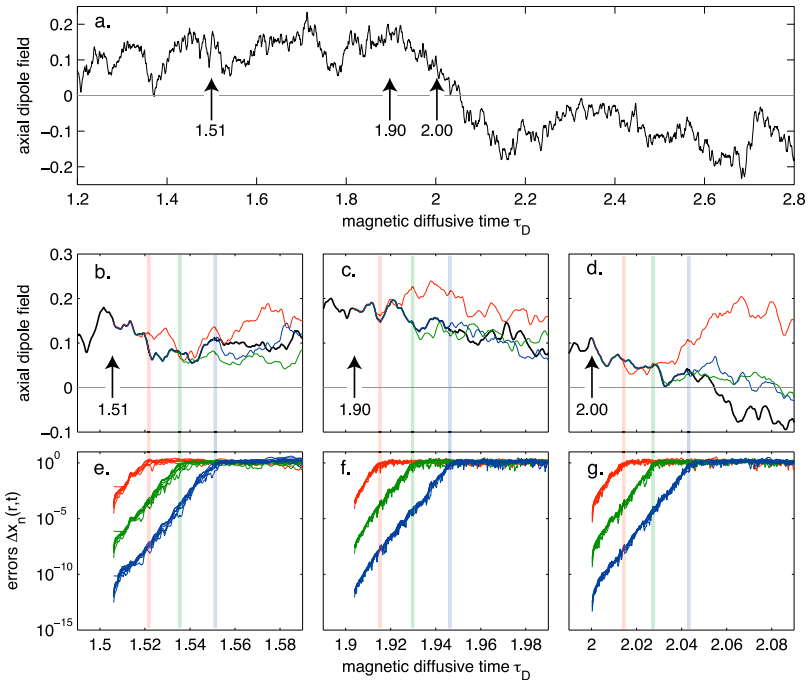

Figure 1. Error growth in a perturbed dynamo simulation. In this example (with $E = 10^{-3}$, $Pr = 1$, $Pm = 10$ and $Ra^* = 0.6$, leading to $Rm \approx 500$), perturbations of three different relative magnitudes ($\varepsilon = 10^{-2}$, red; $\varepsilon = 10^{-6}$, green; and $\varepsilon = 10^{-10}$, blue, same color codes in all plots) have been introduced in the axial dipole at three different times (as indicated by black arrows). (a) The axial dipole field at the core surface for the reference run is shown (arbitrary scale) as a function of time (scaled in units of $\tau_D \approx 120$ kyr). Close-ups also show the diverging evolution of the axial dipole field once the perturbation has been introduced at time (b) $t_p = 1.51\ \tau_D$, (c) $t_p = 1.90\ \tau_D$ or (d) $t_p = 2.00\ \tau_D$. Introducing a perturbation in the axial dipole also affects all other physical fields: shown here on a semi-logarithmic scale, all spherical harmonic degrees (up to $n = 8$) (e) of the poloidal magnetic field at the core surface, and (f) of the poloidal flow and (g) temperature fields at mid-fluid core depth (as computed from the corresponding $\Delta x_n(r, t)$, see text), each plot corresponding to a different value of t_p. Color-coded vertical bars mark the times when the perturbed solutions start behaving in a way totally unrelated to the reference solution.

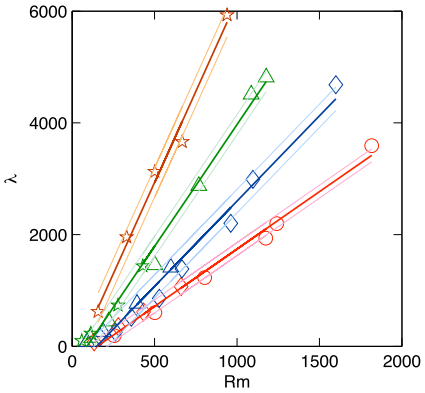

Figure 2. Error growth rate λ as a function of the magnetic Reynolds number Rm. All simulations have been run with the Earth-like value $Pr = 1$. Different colors correspond to different Ekman numbers: $E = 10^{-3}$, red; $E = 3 \times 10^{-4}$, blue; $E = 10^{-4}$, green; $E = 3 \times 10^{-5}$, brown. Different symbols correspond to different range of magnetic Prandtl numbers: $Pm = 0.5 - 1$, stars; $Pm = 2 - 3$, triangles; $Pm = 5 - 9$, diamonds; $Pm = 10 - 15$, circles. For each value of E, a best linear fit is also plotted with 1σ limits (light lines). Note that all $E = 3 \times 10^{-5}$ simulations have only been run with $Pm = 0.5 - 1$ and for numerically accessible $Rm < 1000$.

$x_n^m(r, t_p)(1 + \alpha_n^m \varepsilon)$, each α_n^m being an independent draw from a zero mean unit variance normal law). Each perturbed solution was next restarted, and compared to the reference solution. Logarithmic plots of $\Delta x_n(r,\ t) = \sqrt{\frac{1}{2n+1}\sum_{m=0}^{n}\frac{\left(\tilde{x}_n^m(r,t)-x_n^m(r,t)\right)^2}{\left\langle x_n^m(r)\right\rangle^2}}$ (where $\langle x_n^m(r)\rangle$ stands for the RMS value of the $x_n^m(r,\ t)$ time series) were finally used to infer the perturbation growth rate as seen in each degree n of the magnetic, flow or temperature fields at various radii within the core.

[10] Figure 1 illustrates the consequence of introducing such perturbations at any of three different times in one reference run. In all cases, the perturbed simulation first follows the reference solution closely, but always eventually evolves in a totally unrelated way. The larger the perturbation, the sooner the divergence occurs. Plotting the difference between the perturbed and reference solutions on a semi-logarithmic scale clearly shows that this difference is always growing in the same exponential manner. For each reference run we similarly ran a large number of tests and checked that this behavior was always found, independently of the time and the way the initial perturbation was introduced (be it in the magnetic, flow, or temperature fields involved in the equations governing the dynamo), and independently of the parameter used to monitor the subsequent evolution of the simulations (again, magnetic, flow, or temperature fields). For each reference simulation, always the same error growth rate was recovered, to within roughly 20% fluctuations. From this we infer that each reference simulation, and hence each set of control parameters E, Pr, Pm and Ra^*, is associated with a single dominant error growth rate, which we define as $\lambda = \tau_e^{-1}$, where τ_e is the e-folding time of the exponential growth.

4. Scaling Rules for the Error Growth Rate

[11] The universal character of the error growth rate we observe suggests that it is directly related to the advection of the error fields by the background dynamo flow, which indeed advects all fields (magnetic, temperature and the flow itself) in a similar manner. This in turn suggests that the error growth rate λ is scaled by the inverse of the turnover time $\tau_T = D/U_0$, and is therefore proportional to $Rm = \tau_D / \tau_T$ when measured in units of the known quantity τ_D^{-1}. Figure 2 shows that this is indeed the case. Figure 2 however also shows that the proportionality factor is sensitive to the value of E, which we further interpret in terms of a geometrical effect of the leading scales of the background dynamo convection. Advection of the field by the dynamo flow is also known to govern the timescales τ_n that characterize the time variations of each non-dipole spherical harmonic degree

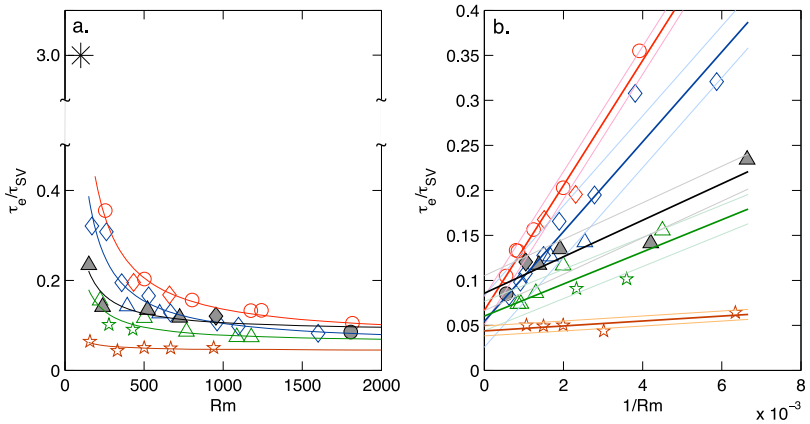

Figure 3. Ratio τ_e / τ_{SV} of the error growth e-folding time τ_e to the characteristic timescale τ_{SV} (computed following *Christensen and Tilgner* [2004]), (a) as a function of the magnetic Reynolds number Rm, and (b) as a function of $1/Rm$. Same color-coding and symbols as in Figure 2. For each value of E, a best linear fit is also plotted with 1σ limits (light lines) in Figure 3b, with corresponding curves reported in Figure 3a. Also shown are τ_e / τ_{SV} ratios for six compositionally driven dynamo simulations computed as by *Olson et al.* [2009], with $E = 3 \times 10^{-4}$, $Pr = 1$ and $Pm = 3 - 12$ (filled black symbols, linear fit with 1σ limits in black lines), and for the high E and low Rm compositionally driven dynamo specifically investigated by *Olson et al.* [2009] (large star).

n of the (observable) field at the core surface (defined as $\tau_n = \left[\left\langle \sum_{m=0}^{n} \left(g_{nm}^2 + h_{nm}^2 \right) \right\rangle \Big/ \left\langle \sum_{m=0}^{n} \left(\dot{g}_{nm}^2 + \dot{h}_{nm}^2 \right) \right\rangle \right]^{1/2}$, where g and h are the Gauss coefficients of the field, the dot marks their time derivative and $\langle\ \rangle$ the time average [see *Hulot and Le Mouël*, 1994; *Christensen and Tilgner*, 2004]). Indeed, in numerical simulations as well as for the Earth's magnetic field, those follow a $\tau_n = \tau_{SV} / n$ law to within a reasonable approximation, with τ_{SV}^{-1} (again measured in units of the known quantity τ_D^{-1}) being mainly proportional to Rm. This common main dependence of $\lambda = \tau_e^{-1}$ and τ_{SV}^{-1} on Rm finally suggests that we also plot the ratio τ_e / τ_{SV} as a function of Rm. Figure 3 shows that for high Rm (low $1/Rm$), τ_e / τ_{SV} converges towards a constant value, fairly independently of the exact value of E (at least within the range $E = 10^{-3} - 10^{-5}$ of values reasonably accessible for such a multi-run numerical study, and close to the $E = 10^{-6}$ value currently achieved in the most advanced dynamo simulations [*Kageyama et al.*, 2008; *Christensen et al.*, 2009]). This convergence is achieved all the faster as E is small.

5. Consequences for Earth's Dynamo Predictability

[12] Given that, as we saw, $E < 10^{-9}$ and $Rm > 100$ for the geodynamo, Figure 3 suggests a maximum value of $\tau_e \approx 0.05\tau_{SV}$ for the Earth's main magnetic field. Using $\tau_{SV} = 535$ yr [*Christensen and Tilgner*, 2004] then leads to an e-folding time of $\tau_e \approx 30$ yr, and a doubling time of roughly 20 years, analogue of the 1.5 days doubling time in meteorology [*Kalnay*, 2003].

[13] These results have several important implications. They first show that, provided the physics of the geodynamo is properly captured by such codes, data assimilation strategies based on 3D dynamo codes [*Kuang et al.*, 2008] could significantly improve on current simple linear temporal extrapolations of the field [*Maus et al.*, 2005]. Satellite data now make it possible to know the main magnetic field within 10–20 nT at the Earth's surface (the average magnitude of the field being on order 40,000 nT). But linear extrapolations typically lead to errors on order 100 nT after just five years [*Maus et al.*, 2008]. Our results thus suggest that using an ideal assimilation scheme could lead to a prediction of similar quality after 50 to 70 years (as inferred from $\tau_e \approx 30$ yr times ln(100/20) or ln(100/10)). In fact, the evolution of large-scale structures (such as the South Atlantic Anomaly, which does not need to be known to much better than 10% error for most applications [*Heirtzler*, 2002]) might even be predictable beyond that range, since in practice (and as also observed in meteorology [*Kalnay*, 2003]), the error growth rate always slackens when errors reach large values (see Figure 1). In contrast, our results also point at the fundamental impossibility of predicting when the next magnetic field reversal will occur. Indeed, in each of our simulations the error growth rate is always the same, even close to a reversal; and once an error has led a perturbed solution to evolve in a way unrelated to the unperturbed solution, information about the timing of the next reversal is also lost (Figure 1d). Since we know from examination of past reversals [*Constable and Korte*, 2006] that the next reversal could not occur before a couple of thousand years, way beyond the century timescale that can possibly be envisioned for any realistic prediction, it thus seems very unlikely that the next reversal could plausibly be predicted.

6. Concluding Comments

[14] All numerical simulations discussed so far are thermally driven, and assume simple boundary conditions. The way Earth's dynamo is driven is likely more complex, and the above extrapolation to Earth's dynamo predictability should therefore be taken with substantial caution. Also, in much the same way progress in numerical modeling has led to a reduction by a factor two of the doubling time in meteorology [see *Kalnay*, 2003], future simulations with more realistic lower Ekman numbers could lead to a lower estimate of the e-folding time than we inferred. However, it is worth noting that additional results from a few simulations based on compositionally (rather than thermally) driven numerical dynamos do bring substantial support to the general character of our findings. Those simulations have been computed following *Olson et al.* [2009], and have also been found to lead to the same type of error growth as those reported above. In particular, and as can be seen in Figure 3, the corresponding τ_e / τ_{SV} ratios again converge towards the same limit value for high Rm. Interestingly, we finally note that in the case of the compositionally driven dynamo investigated in much detail by *Olson et al.* [2009] (with $E = 6.5 \times 10^{-3}$, $Pr = 1$, $Pm = 20$ and $Ra = 1.9 \times 10^4$, where Ra is the compositional Rayleigh number as defined by *Olson et al.* [2009], leading to $Rm \approx 100$), we do find a very high value of $\tau_e/\tau_{SV} \approx 3$ (large star in Figure 3a), showing that such a dynamo is indeed exceptionally predictable, in agreement with these authors' claim that (contrary to dynamos with low E) such a dynamo could display some long-term reversal precursor. Our results however clearly point at Earth's dynamo being unfortunately far less predictable.

[15] **Acknowledgments.** Very helpful comments by Andrew Tangborn and an anonymous reviewer are gratefully acknowledged. This study was supported by the SEDIT programme of CNRS-INSU. Numerical computations were performed at S-CAPAD, IPGP, France and at HPC resources from GENCI-CINES/IDRIS (grant 2009-042122). This is IPGP contribution 2604.

References

Aubert, J., J. Aurnou, and J. Wicht (2008), The magnetic structure of convection-driven numerical dynamos, *Geophys. J. Int.*, *172*, 945–956, doi:10.1111/j.1365-246X.2007.03693.x.

Baker, D. N. (2002), How to cope with space weather, *Science*, *297*, 1486–1487, doi:10.1126/science.1074956.

Charney, J. G., R. G. Fleagle, H. Riehl, V. E. Lally, and D. Q. Wark (1966), The feasibility of a global observation and analysis experiment, *Bull. Am. Phys. Soc.*, *47*, 200–220.

Christensen, U. R., and J. Aubert (2006), Scaling properties of convection-driven dynamos in rotating spherical shells and application to planetary magnetic fields, *Geophys. J. Int.*, *166*, 97–114, doi:10.1111/j.1365-246X.2006.03009.x.

Christensen, U. R., and A. Tilgner (2004), Power requirement of the geodynamo from ohmic losses in numerical and laboratory dynamos, *Nature*, *429*, 169–171, doi:10.1038/nature02508.

Christensen, U. R., and J. Wicht (2007), Numerical dynamo simulations, in *Treatise on Geophysics*, vol. 8, *Core Dynamics*, edited by P. Olson, pp. 245–282, doi:10.1016/B978-044452748-6.00134-6, Elsevier, Amsterdam.

Christensen, U. R., et al. (2001), A numerical dynamo benchmark, *Phys. Earth Planet. Inter.*, *128*, 25–34, doi:10.1016/S0031-9201(01)00275-8.

Christensen, U. R., V. Holzwarth, and A. Reiners (2009), Energy flux determines magnetic field strength of planets and stars, *Nature*, *457*, 167–169, doi:10.1038/nature07626.

Constable, C., and M. Korte (2006), Is Earth's magnetic field reversing?, *Earth Planet. Sci. Lett.*, *246*, 1–16, doi:10.1016/j.epsl.2006.03.038.

Fournier, A., C. Eymin, and T. Alboussière (2007), A case for variational geomagnetic data assimilation: Insights from a one dimensional, nonlinear, and sparsely observed MHD system, *Nonlinear Processes Geophys.*, *14*, 163–180.

Glatzmaier, G. A., and P. H. Roberts (1995), A three-dimensional convective dynamo solution with rotating and finitely conducting inner core and mantle, *Phys. Earth Planet. Inter.*, *91*, 63–75, doi:10.1016/0031-9201(95)03049-3.

Heirtzler, J. R. (2002), The future of the South Atlantic anomaly and implications for radiation damage in space, *J. Atmos. Sol. Terr. Phys.*, *64*, 1701–1708, doi:10.1016/S1364-6826(02)00120-7.

Hulot, G., and J. L. Le Mouël (1994), A statistical approach to the Earth's main magnetic field, *Phys. Earth Planet. Inter.*, *82*, 167–183, doi:10.1016/0031-9201(94)90070-1.

Hulot, G., C. Eymin, B. Langlais, M. Mandea, and N. Olsen (2002), Small-scale structure of the geodynamo inferred from Oersted and Magsat satellite data, *Nature*, *416*, 620–623, doi:10.1038/416620a.

Jones, C. A., N. O. Weiss, and F. Cattaneo (1985), Nonlinear dynamos: A complex generalization of the Lorenz equations, *Physica D*, *14*, 161–176, doi:10.1016/0167-2789(85)90176-9.

Kageyama, A., T. Miyagoshi, and T. Sato (2008), Formation of current coils in geodynamo simulations, *Nature*, *454*, 1106–1109, doi:10.1038/nature07227.

Kalnay, E. (2003), *Atmospheric Modeling, Data Assimilation and Predictability*, 341 pp., Cambridge Univ. Press, Cambridge, U. K.

Kuang, W., A. Tangborn, W. Jiang, D. Liu, Z. Sun, J. Bloxham, and Z. Wei (2008), MoSST_DAS: The first generation geomagnetic data assimilation framework, *Commun. Comput. Phys.*, *3*, 85–108.

Lorenz, E. N. (1963), Deterministic nonperiodic flow, *J. Atmos. Sci.*, *20*, 130–141, doi:10.1175/1520-0469(1963)020<0130:DNF>2.0.CO;2.

Lorenz, E. N. (1965), A study of the predictability of a 28-variable atmospheric model, *Tellus*, *17*, 321–333.

Lundin, R., H. Lammer, and I. Ribas (2007), Planetary magnetic fields and solar forcing: Implications for atmospheric evolution, *Space Sci. Rev.*, *129*, 245–278, doi:10.1007/s11214-007-9176-4.

Maus, S., et al. (2005), The 10th generation international geomagnetic reference field, *Phys. Earth Planet. Inter.*, *151*, 320–322, doi:10.1016/j.pepi.2005.03.006.

Maus, S., L. Silva, and G. Hulot (2008), Can core-surface flow models be used to improve the forecast of the Earth's main magnetic field?, *J. Geophys. Res.*, *113*, B08102, doi:10.1029/2007JB005199.

Olson, P., P. Driscoll, and H. Amit (2009), Dipole collapse and reversal precursors in a numerical dynamo, *Phys. Earth Planet. Inter.*, *173*, 121–140, doi:10.1016/j.pepi.2008.11.010.

Roberts, P. H. (2007), Theory of the geodynamo, in *Treatise on Geophysics*, vol. 8, *Core Dynamics*, edited by P. Olson, pp. 67–105, doi:10.1016/B978-044452748-6.00133-4, Elsevier, Amsterdam.

Ryan, D. A., and G. R. Sarson (2008), The geodynamo as a low-dimensional deterministic system at the edge of chaos, *Europhys. Lett.*, *83*, 49001, doi:10.1209/0295-5075/83/49001.

J. Aubert, Equipe de Dynamique des Fluides Géologiques, Institut de Physique du Globe de Paris, Université Paris-Diderot, INSU, CNRS, 4, place Jussieu, Case 89, F-75252 Paris CEDEX 05, France.

G. Hulot and F. Lhuillier, Equipe de Géomagnétisme, Institut de Physique du Globe de Paris, Université Paris-Diderot, INSU, CNRS, 4, place Jussieu, Case 89, F-75252 Paris CEDEX 05, France. (gh@ipgp.fr)